Geol. Mag. **143** (*2*), *2006, pp. 181–193. © 2006 Cambridge University Press*
doi:10.1017/S0016756806001713 *Printed in the United Kingdom*

Metasedimentary xenoliths in the lavas of the Timanfaya eruption (1730–1736, Lanzarote, Canary Islands): metamorphism and contamination processes

A. APARICIO*, M. A. BUSTILLO, R. GARCIA & V. ARAÑA

Museo Nacional de Ciencias Naturales (CSIC), c/ José Gutiérrez Abascal 2, 28006 Madrid, Spain

(*Received* 14 December 2004; *accepted* 27 September 2005)

Abstract – We report on the investigation of contact metamorphism provoked by the emplacement of a shallow magma chamber during the Timanfaya eruption of Lanzarote from 1730 to 1736 AD. The study was carried out on metamorphic xenoliths from basaltic Timanfaya lavas, and shows how the primary basanitic magma was contaminated by sedimentary and metamorphic rocks. Mineralogical and chemical studies allowed the definition of several xenolith types. Silica xenoliths (quartz, tridymite, cristobalite or a mixture of these, constituting more than 50 % of the xenolith) and calc-silicate xenoliths (wollastonite, sometimes the 2M type, diopside, forsterite or mixture of these, constituting more than 50 % of the xenolith) are the most frequent. Other minerals recognized were calcite, dolomite, augite, enstatite, hypersthene, spinel and scapolite. The mineralogy and some textures of the metamorphic forsteritic xenoliths are identical to those found in ultrabasic xenoliths (dunites) and point to a possible metamorphic origin for some of them. Major and trace elements showed a diversity of composition, controlled by the mineralogy. The REE composition of the metamorphic xenoliths is high, compared with the sedimentary xenoliths not affected by metamorphism. The mineral assemblages define metamorphic facies of low, medium and high grade, depending on the distance of the sedimentary rocks from the magma chamber border. The IGPETWIN-MIXING program was used to verify the contamination process, taking the xenoliths as representative of the sedimentary/metamorphic rocks that were melted. The results indicated that sedimentary/metamorphic rock contamination of a basanitic magma can produce tholeiitic compositions.

Keywords: metasedimentary xenoliths, contact metamorphism, assimilation, tholeiitic basalts.

1. Introduction

The Timanfayaeruption (1730–1736), the longest recorded in the Canary Archipelago (Fig. 1), was characterized by basaltic flows with tholeiitic tendencies. Unlike the predominantly basanitic composition of most rocks from recorded Canary Island eruptions, Timanfaya lavas are relatively enriched in silica (Ibarrola & López Ruiz, 1967; Ibarrola, 1970; Brandle & Fernández-Santín, 1979).

Petrogenetic aspects of the Timanfaya magma led Carracedo & Rodríguez-Badiola (1991) to suggest that the composition of basanite, basalt and tholeiitic rock lavas indicates magma formation at depths of 15 to 70 km; at 70 km, low melting rates would segregate basanites; at 35–70 km, and with moderate melting rates, alkaline basalts would form; at 15–35 km with high melting rates, tholeiitic basalts would form. In addition, Sigmarsson, Carn & Carracedo (1998) inferred that the variation in the composition of the magma may be due to different degrees of melting of lherzolite and suggested that 200 years were required for the transport of the magma to the surface. Thomas *et al.* (1999) described some isotopic anomalies and minor element variations in the recent lavas of Lanzarote, which they consider to have been produced by a mixing process in which the end members correspond to magmas generated at different depths of the melt column.

Ortiz *et al.* (1986) detected a cooling magma reservoir at a depth of 4 km, related to the Timanfaya eruption. Araña & Bustillo (1992) attribute the contamination and enrichment in silica of this shallow reservoir to the mixture of its primary magma with melted silica-rich sedimentary rocks (mainly radiolarites).

Ultrabasic xenoliths, mainly dunites, have been found in the lavas of the 1730–1736 eruption (Sagredo, 1969; Neumann *et al.* 1995). According to Sagredo (1969), although basalts and dunites came from the mantle, they cannot be considered to be cogenetic, given their chemical and structural differences. Neumann *et al.* (1995) classified the xenoliths similarly to Sagredo (1969), also with a mantle origin, although they pointed to a possible metasomatism there.

Other xenoliths, of sedimentary origin, are calc-silicate and silica rocks, and to a lesser extent sandstones, limestones and claystones (Ortiz, Araña & Valverde, 1986; Araña & Ortiz, 1991; Araña & Bustillo, 1992; Bustillo *et al.* 1994). Extensive sampling and study of Timanfaya sedimentary xenoliths

*Author for correspondence: mcny144@mncn.csic.es

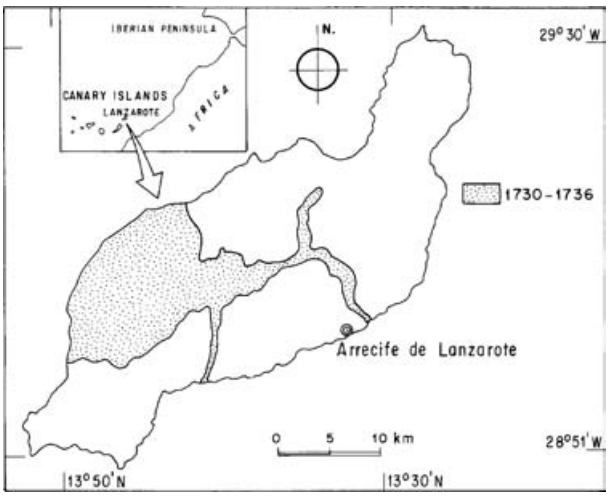

Figure 1. Schematic view of Lanzarote Island showing the location of 1730–1736 Timanfaya lava eruptions.

(most ofthem metamorphosed) are presented in this paper. The xenoliths are found throughout flows of the studied area (Fig. 1). Most of the xenolith samples come from the lavas emitted in the late stages of the 1730–1736 eruption (Carracedo & Rodríguez-Badiola, 1991).

This work attempts to define metamorphic conditions through an in-depth study of various types of metamorphosed xenoliths, with various mineral assemblages and their chemical compositions. The host magma relationship with xenoliths is analysed to determine the extent of contamination of a primary basanitic magma by melting of rocks hosting the magma chamber.

The Canary Island crust has been extensively studied (Banda *et al.* 1981, 1992; Suriñach, 1986; Ranero & Banda, 1997; Watts, 1994; Watts *et al.* 1997; Schmincke *et al.* 1998; Collier & Watts, 2001; Krastel & Schmincke, 2002). At Lanzarote the crust is 11 km thick (Suriñach, 1986). Figure 2 is a schematic view of the main sections of the crust, derived from data obtained in previous studies. A geothermic bore-hole drilled at Lanzarote (2700 m deep) reached the base of the volcanic shield at 2598 m, underlain only by sedimentary rocks (Sánchez Guzmán & Abad, 1986). These rocks were described as cross-stratified sandstones, micrites containing silica, cherts, clays and marls, some containing microfauna of the Middle and Upper Palaeocene. These sedimentary rocks, together with those underlying them, correlate with those located in the east Lanzarote basin (Martínez & Buitrago, 2002). The total thickness of the sedimentary beds in the upper crust below Lanzarote may be taken to be about 2 km, given the low seismic velocity (4 km s^{-1}) in the upper 4–5 km of the crust (Banda *et al.* 1992).

The complexity of the Jurassic–Cretaceous to Miocene sedimentary series can be seen in neighbouring

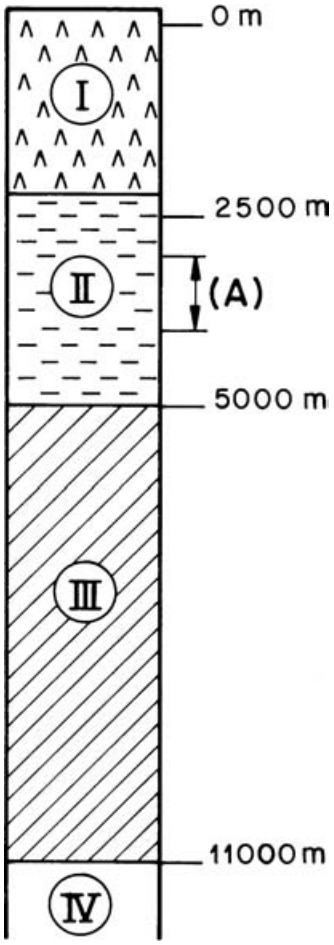

Figure 2. Schematic view of Lanzarote substrate from geothermic drill data, from as deep as 2500 m below sea level (Sánchez & Abad, 1986), from petroleum prospecting east of Lanzarote (Martínez & Buitrago, 2002) and from studies of the seismic velocity in the crust (Banda *et al.* 1981; Suriñach, 1986). Also included is the position of a cooling magma chamber (A), detected in various studies and located with a magnetotelluric survey at 3 to 4 km depth (Ortiz *et al.* 1986). (I) Volcanic shield (mainly submarine tuffs). (II) Upper crust (4 km s^{-1}) (sedimentary rocks from Paleocene to Lower Cretaceous). (III) Lower crust (5.9 km s^{-1}). (IV) Upper mantle.

Fuerteventura (Robertson & Bernoulli, 1982; Renz, Bernoulli & Hottinger, 1992) and along the African continental border (De Ros, Morad & Al-Aasm, 1997). Within these series, these authors cite lithologies as diverse as mudstones, quartz lutites, slates, siltstones, sandstones (frequently orthoquarzites), marls, limestones (rich in silica, and containing nodules of chert) and dolomites. From the most ancient metasedimentary rocks (Lower Cretaceous: Renz, Bernoulli & Hottinger, 1992) cropping out in the Basal Complex of Fuerteventura, some authors (Fuster *et al.* 1968; Stillman *et al.* 1975) have deduced evidence of regional metamorphism. They describe greenschist facies with a geothermal gradient of 45 °C km^{-1} (De Ros, Morad & Al-Aasm, 1997).

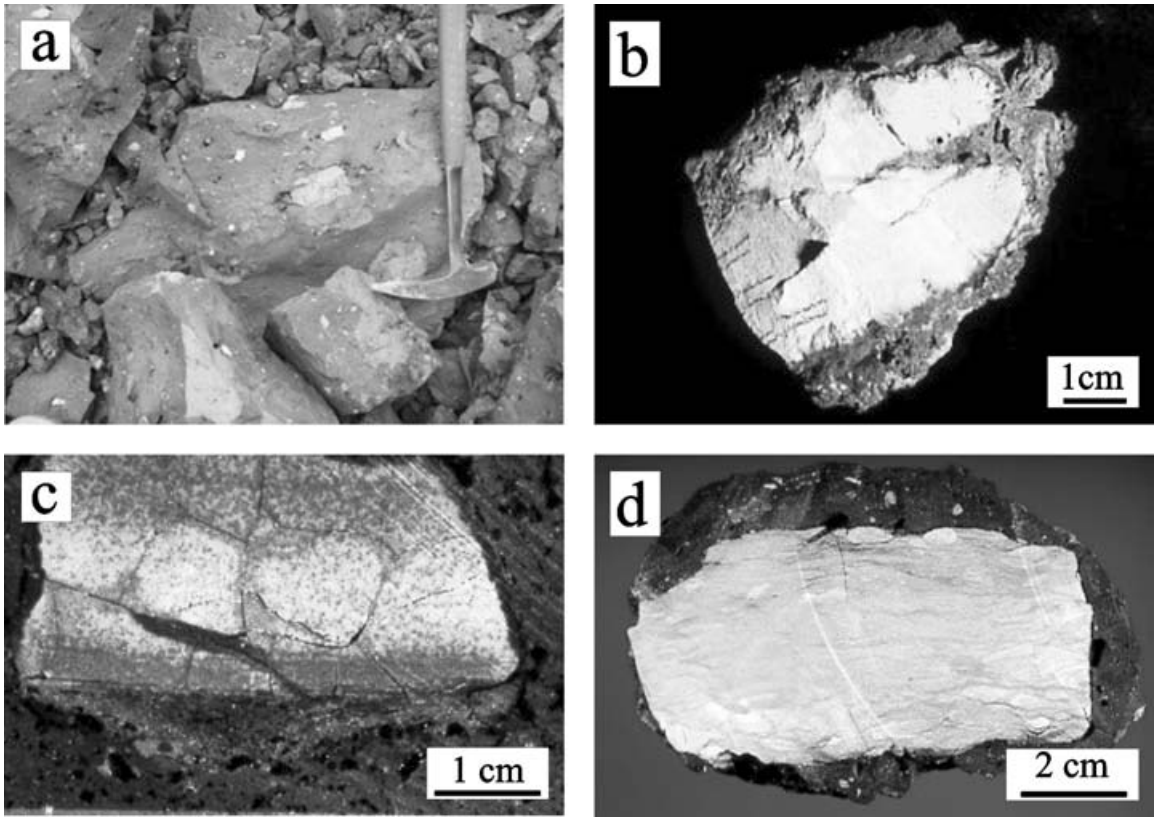

Figure 3. Features of xenoliths. (a) Xenoliths contained in several boulders of lava flows in a quarry. They are white or beige and their size rarely exceeds 12 cm. (b) Xenolith with massive structure. The volcanic host rock penetrates through cracks. (c) Xenolith with isolated crystals and relics of sedimentary structure. (d) The largest xenolith found with sedimentary structures, corresponding to sample ANG-31, made up of quartz, wollastonite 2M and calcite.

2. Methodology

Mineralogy was determined by light microscopy and by X-ray diffraction (XRD) in the laboratories of the Museo Nacional de Ciencias Naturales (MNCN) using a Philips semi-automatic PW 1710 diffractometer, plus mineral identification programs (Carbonin & Menegazzo, 1996). Major elements were determined by Perkin-Elmer 2380 atomic absorption spectroscope in the same laboratories; minor, trace and lanthanide elements were analysed by ICP-MS at CNRS (Nancy, France) according to the method of Govindaraju & Mevelle (1987). The composition of the minerals was determined using a JEOL JXA-8900 M automatic electronic microprobe with an EPMA, using WDS, to 15 kv and 20 nA, at the Electronic Microscopy Laboratory of Universidad Complutense (Madrid, Spain). The standards used are described by Jarosewich, Nelen & Norberg (1980) and were provided by the Smithsonian Institute (Washington DC, USA).

The isotopic composition of Sr was determined on a Finnigan MAT-261 eight-collector mass spectrometer. The separation of Sr by isotope analyses was performed following the methods of Richard, Shimizu & Allegre (1976).

3. Petrology

The metasedimentary xenoliths are small, round to subround, with longest dimension from 1 mm to 12 cm, and appear homogeneously distributed in the lava, usually with a cryptocrystalline to microcrystalline texture (Figs 3, 4). Bustillo *et al.* (1994) described characteristics in some of them that denote the existence of sedimentary structures, including fine stratification, current ripples, erosive contacts and detrital grains, etc., which have almost completely disappeared where there has been a high degree of thermal transformation. In less-transformed xenoliths, radiolarians and other microfossils are also observed, some of them indicating a Late Palaeocene age (Bustillo *et al.* 1994).

According to the mineralogy obtained by XRD (Table 1), there are two main types of xenoliths: silica (quartz, tridymite, cristobalite or a mixture of these constitute more than 50 % of the silica xenoliths), and calc-silicate (wollastonite, sometimes the 2M type, diopside, forsterite or a mixture of these constitute more than the 50 % of the calc-silicate xenoliths), although transitional types with calc-silicate and silica minerals are frequent. Small amounts of calcite and dolomite can appear sporadically in silica xenoliths, but are more common in calc-silicate xenoliths. Occasionally

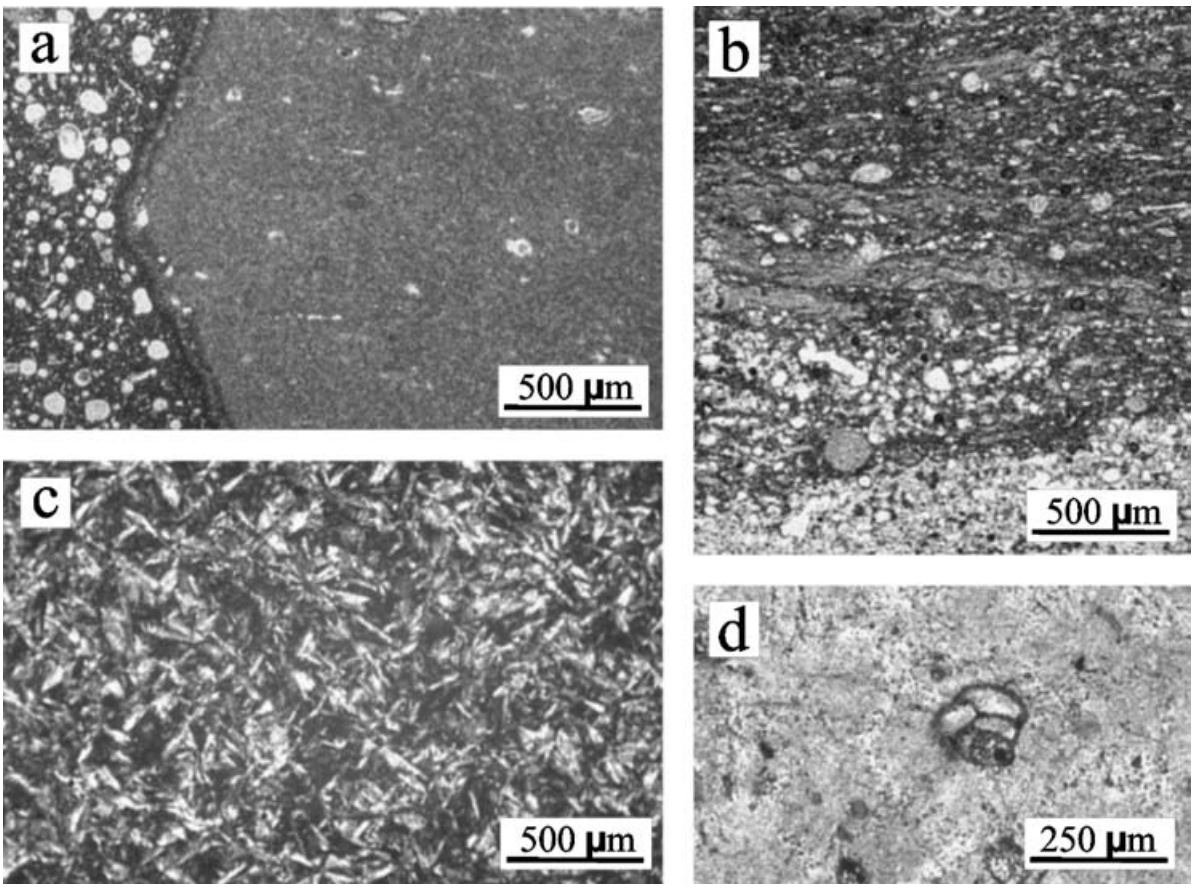

Figure 4. Photographs of texture and mineralogical details of xenoliths. (a) Contact between a cryptocrystalline calc-silicate (right) and the basalt (left) xenolith. Parallel nicols. (b) Radiolarian ghosts and laminations in a metamorphic silica xenolith composed mainly of quartz, cristobalite and wollastonite. Parallel nicols. (c) Metamorphic silica xenoliths composed of tridymite. The tridymite crystals are rectangular or wedge-shaped and are sometimes arranged in aggregates. Crossed nicols. (d) Close-up of a tridymitic xenolith with ghost of microforaminifers and other microfossils. Parallel nicols.

small amounts of moganite (a silica polymorph with a bonding similar to that of quartz: Heaney & Post, 1992) are present in silica xenoliths, although their determination by XRD is difficult due to the interference of moganite with quartz. In a metamorphic pelitic rock, the main minerals found are quartz and phyllosilicates (illite).

Under light microscopy, the xenolith–volcanic rock contact is sharp, and in some cases the outer part of the xenolith is weakly altered (Fig. 4a). The quartz appears as crystals of various sizes (30–120 μm), and many, especially those of rounded shape, may be detrital grains. Different degrees of melting of quartz and interstitial glass can be seen in some silica xenoliths.

The texture of the cristobalite, wollastonite and diopside is microcrystalline or cryptocrystalline (Fig. 4a, b). Rectangular or wedge-shaped tridymite crystals of various sizes up to 100 μm, in some cases arranged in aggregates (rosettes) (Fig. 4c), are seen. Ghosts of radiolarians and other microfossils (Fig. 4b, d) can be seen in silica and calc-silicate xenoliths.

Texture of forsterite included in the metasedimentary xenoliths varies from microcrystalline to cryptocrystalline (Fig. 5a), but zones of phenocrysts in a microcrystalline groundmass (Fig. 5b) are also found, while in other cases the microcrystalline groundmass is lacking and only phenocrysts with undulose extinction are found (Fig. 5c). This latter type of forsteritic xenolith is very similar to the ultrabasic xenoliths from the mantle (Sagredo, 1969; Neumann *et al.* 1995) but it is lighter in colour than the typical dunitic xenoliths.

In the microprobe (Table 2), complex mineral assemblages of clinopyroxene (diopside, augite), orthopyroxene (enstatite and hyperstene) and olivine (forsterite) are detected in some xenoliths. The orthopyroxenes and forsterite also appear associated with spinel (chromite). Another calc-silicate mineral, scapolite, was also identified.

The diversity of minerals in xenoliths indicates varying degrees of metamorphism, ranging from unaffected sedimentary rocks to those in which the original texture and mineralogy have been completely altered.

Table 1. Xenolith mineralogical composition determined by XRD

Minerals	Q	Tr	Cb	Di	Wo	Fo	Ca	Do	Others
Metamorphic silica rocks									
ANG-76	∗	++++							
ANG-89		++++							
ANG-81	+	++++							
ANG-87	∗	++++	∗						
ANG-58	+++		++						
ANG-39	+++		++						
ANG-19	++++		+						Phy (∗)
ANG-74	+		++++						
ANG-26	+		++++						Phy (∗)
ANG-17	++++								Fd (∗)
ANG-41	++++		+	+					
ANG-20	+		+++	+					
ANG-32	++++			+					Pl (∗)
ANG-100	+++			++				++	
ANG-24	++		+	++	++				Pl (∗)
ANG-54	++		++	∗	++				
ANG-31	+++				+ (2M)		+		
ANG-93	+		+++		+ (2M)		∗		
Metamorphic calc-silicate rocks									
ANG-59					++++ (2M)				
ANG-40	+				++++(2M)				
ANG-43	+				++++		∗		
ANG-71	+		++		+++ (2M)				
ANG-18					++++				
ANG-86			++		++			∗	Pl (∗)
ANG-83			++		++				
ANG-12			++		+++				
ANG-64	∗		∗	∗	+++				
ANG-46				∗	++++ (2M)		∗		
ANG-37	+			∗	++++				
ANG-6	++			+++					
ANG-77	+			++++					
ANG-73	∗			++++			∗		Pl (∗)
ANG-15	+			++++				+	
ANG-29						++++			
ANG-23						++++			Hy (+)
Metamorphic pelitic rock (slate)									
ANG-42	+++								Ill (++)
Sedimentary rocks (radiolarite and limestone)									
ANG-17	++++						+		Fd (+)
ANG-11							++++		Br (+)

Fd – Alkali feldspar; Br – Brucite; Ca – Calcite; Cb – Cristobalite; Di – Diopside; Do – Dolomite; Fo – Forsterite; Hy – Hypersthene; Ill – Illite; Phy – Phyllosilicates; Pl – Plagioclase; Q – Quartz; Tr – Tridymite; Wo – Wollastonite; Wo2M – Wollastonite 2M. Amounts in % wt: (++++ >75); (+++ 75–50); (++ 50–25); (+ 25-10); (∗ <10).

Table 2. Selected xenolith mineral assemblages determined by microprobe

Sample	Calc-silicate rock
ANG-120	Fo+En+Cr
ANG-96	Fo+En+Di
ANG-121	Fo+Sc+Cr
ANG-37	Wo+Qz+Di
ANG-122	Fo+Au
ANG-123	Fo+Au+Pc
ANG-124	Fo+Au-Di
ANG-125	Fo+Au+Sc
ANG-126	Fo+En
ANG-101	Fo+Cr
ANG-46	Wo+Ca+Di
ANG-97	Sc+Qz+Or
ANG-9	Fo+Cr

Au – Augite; Ca – Calcite; Cr – Chromite; Di – Diopside; En – Enstatite; Fo – Forsterite; Or – Orthoclase; Pc – Periclase; Q – Quartz; Sc – Scapolite; Wo – Wollastonite

4. Geochemistry of xenoliths and minerals

A representative sub-set of xenoliths was analysed to determine major and trace elements (Table 3). Silica and calc-silicate xenoliths were distinguished mainly according to their amount of silica. Of the silica xenoliths, those whose silica mineral is tridymite are richer in silica than those composed of cristobalite and quartz. Anomalous amounts of Al_2O_3 were detected in cristobalitic/quartz xenoliths, part of which correspond to the phyllosilicates, while the other part may come from the cristobalite itself (Smith & Steele, 1984).

Calc-silicate xenolith composition is very variable due to the many types of calc-silicate minerals varying significantly in CaO, MgO, Al_2O_3 and Fe_2O_3 amounts. In mono-mineral xenoliths containing wollastonite

Table 3. Chemical composition of selected calc-silicate and sedimentary xenoliths (oxides in wt %)

Sample	ANG-29	ANG-64	ANG-46	ANG-37	ANG-59	ANG-73	ANG-18	ANG-43	ANG-12	ANG-96	ANG-83	ANG-77	ANG-6
SiO_2	44.22	46.00	49.00	49.41	51.92	56.00	56.57	58.49	59.93	61.14	62.74	62.99	67
TiO_2	0.02	0.35	0.17	0.53	0.14	0.50	0.18	0.2	0.12	0.04	0.16	0.5	0.45
Al_2O_3	0.33	8.20	2.38	10.03	3.22	12.05	3.07	5.52	2.92	1.44	5.10	10.56	9.22
Fe_2O_3	1.42	2.56	0.64	4.82	1.09	5.41	1.01	2.67	0.92	4.92	1.02	4.46	4.18
FeO	7.07	–	–	–	–	–	–	–	–	2.68	0.40	–	–
MnO	0.21	0.12	0.06	0.03	–	0.04	–	0.06	–	0.21	0.09	0.39	0.32
MgO	41.89	2.44	2.42	3.39	0.99	3.58	1.00	1.89	0.9	15.52	2.61	7.02	6.35
CaO	1.94	34.96	38.84	24.73	38.68	16.78	36.56	20.81	30.4	12.72	23.43	8.76	8.2
Na_2O	0.09	1.31	0.12	1.03	0.61	1.26	0.58	1.17	0.56	0.45	0.43	1.07	0.98
K_2O	0.04	0.62	0.15	1.72	0.57	2.20	0.58	0.63	0.51	0.22	0.43	2.24	2.04
P_2O_5	0.05	0.41	0.22	0.43	0.5	0.14	0.30	0.98	0.47	0.04	0.45	0.29	0.09
LOI	2.5	2.87	6.01	3.58	1.99	1.68	–	7.28	3.02	0.46	2.52	1.49	0.95
Total	99.79	99.84	100.0	99.7	99.71	99.64	99.85	99.7	99.75	99.84	99.38	99.77	99.78
Sc				14.3	10.1			12.1	10.5			12.1	11.1
Ba				393	227			292	199			310	290
Be				0.13	0.6			0.29	–			1.16	–
Co				11.7	2.09			17.2	1.84			8.45	13.9
Cr				129	112			333	104			113	79.6
Cu				62.5	35.7			116	35.3			39.5	29.7
Nb				9.75	2.74			4.47	2.5			9.96	8.09
Ni				74.6	39.1			112	39.7			45.1	47.7
Rb				92.4	26.0			28.3	24.0			7.8	79.0
Sr				575	1201			691	1047			234	198
V				154	70.4			112	65.8			97.9	81.0
Y				35.3	15.9			44.0	14.9			29.0	14.3
Zn				132	70.6			312	65.0			74.1	83.7
Zr				227	49.8			44.8	44.3			136	113
La				32.69	13.34			28.3	11.97			25.85	14.19
Ce				53.02	16.43			26.86	14.57			47.04	32.58
Pr				7.38	2.8			5.71	2.51			6.09	4.16
Nd				29.31	11.0			23.27	9.86			24.37	16.34
Sm				5.83	2.32			4.59	1.89			5.09	3.59
Eu				1.26	0.557			1.14	0.468			1.09	0.73
Gd				5.28	2.05			4.59	1.739			4.34	2.52
Tb				0.83	0.314			0.76	0.254			0.68	0.4
Dy				5.08	1.916			4.79	1.775			4.1	2.506
Ho				1.12	0.445			1.17	0.385			0.98	0.556
Er				2.87	1.107			2.99	1.001			2.52	1.456
Tm				0.43	0.178			0.46	0.148			0.42	0.248
Yb				2.8	1.172			2.95	1.03			2.79	1.7
Lu				0.42	0.2			0.46	0.164			0.47	0.244
$^{87}Sr/^{86}Sr$				–	–			–	0.70801			–	–

or wollastonite 2M (samples ANG-18 and ANG-59, respectively; Table 3), or in xenoliths constituted mainly of these minerals (ANG-46 and ANG-64, Table 3), chemical analyses revealed a composition with high Al_2O_3 relative to data published for typical wollastonites (from 0.26 to 0.85 wt % Al_2O_3: Deer, Howie & Zussman, 1992).

The calc-silicate xenoliths present a variable and enriched composition in both heavy and light REEs, compared with the carbonate sedimentary xenolith (biomicrite) (Fig. 6). Within the silica xenoliths, the tridymitic xenolith REE composition falls between that of the calc-silicate xenoliths and the sedimentary xenoliths. The tridymitic xenoliths have a strong negative Ce anomaly that is weak in some calc-silicate xenoliths, and practically non-existent in cristobalitic/quartz xenoliths (Fig. 6). This anomaly is characteristic of marine sediments (Fleet, 1984; Zou *et al.* 2004).

In three cases, isotopic determinations ($^{87}Sr/^{86}Sr$) were made to confirm the sedimentary origin of these xenoliths.

Electron microprobe studies to determine the mineral composition of selected meta-sedimentary samples are difficult in some cases because of cryptocrystalline mineral textures. Nevertheless, clinopyroxenes (wollastonite and diopside), orthopyroxenes, olivines, quartzes, spinels (chromites) and scapolite (Table 4) were identified. The wollastonites have an excess of Al_2O_3 (as was also found in the analyses of whole rock; Table 3); the excess of MgO in sample ANG-46 may be explained by interference of two minerals (wollastonite and diopside) in the analysis, due to the cryptocrystalline texture of the xenolith. The orthopyroxene found is enstatite. The olivines are strongly magnesian (Fo, 84–94 %) and include chrysolite and forsterite types, some with high levels of chromium.

Table 3. (cont.)

Sample	ANG-31	ANG-100	ANG-20	ANG-41	ANG-74	ANG-58	ANG-19	ANG-39	ANG-26	ANG-87	ANG-89	ANG-81	ANG-76	ANG-42(∗)	ANG-11(∗)
SiO_2	66.67	72.30	74.17	74.74	82.00	83.48	84.76	85.51	92.48	93.81	95.00	97.28	97.50	71.39	0.83
TiO_2	0.17	0.39	0.25	0.33	0.27	0.36	0.35	0.42	0.13	0.02	0.13	–	–	0.45	0.02
Al_2O_3	3.97	9.63	6.47	6.78	5.67	7.05	7.60	7.40	3.06	0.74	1.19	0.45	0.49	9.64	0.09
Fe_2O_3	0.98	1.04	1.90	2.86	2.12	2.35	2.78	–	0.91	0.22	0.18	0.18	0.20	4.61	0.3
FeO	0.52	2.29	0.57	–	–	–	–	–	–	–	–	–	–	–	–
MnO	0.04	0.20	0.24	0.37	0.37	0.05	0.02	0.03	0.01	–	–	–	–	0.1	0.02
MgO	1.84	4.56	5.00	5.13	0.60	2.25	2.92	3.30	0.33	0.09	0.14	0.04	0.10	3.1	10.22
CaO	16.96	5.54	8.62	6.4	5.36	1.31	0.27	0.21	0.82	3.24	2.32	0.17	0.23	2.09	45.41
Na_2O	0.36	0.54	0.52	0.88	0.74	0.76	0.92	0.92	0.97	0.25	0.11	0.15	0.15	0.94	–
K_2O	1.40	1.60	1.46	1.34	1.29	1.5	1.70	1.45	0.37	0.06	0.13	0.05	0.07	2.01	–
P_2O_5	0.20	0.20	0.04	0.07	0.15	0.09	–	0.01	0.42	0.36	0.30	–	–	0.37	0.14
LOI	6.88	0.96	0.50	0.91	0.63	0.6	–	0.70	–	0.53	0.37	0.39	0.30	5.1	42.84
Total	99.99	99.56	99.74	99.81	99.20	99.8	101.32	99.97	99.50	99.31	99.87	98.7	99.04	99.8	99.88
Sc				8.8		5.6				3.1		0.7		7.8	9.3
Ba				293		330				212		59.0		313	14.5
Be				–		0.6				–		0.28		0.08	–
Co				5.05		5.29				0.71		0.53		7.61	1.09
Cr				62.2		62.9				41.0		14.0		108	5.9
Cu				14.0		10.2				15.6		4.7		66.0	8.22
Nb				6.57		6.78				0.58		0.28		8.66	1.35
Ni				26.7		25.6				14.8		3.54		47.1	18.0
Rb				57.4		56.8				3.3		2.86		81.3	1.56
Sr				166		127				120		15.9		190	397
V				60.3		57.5				16.0		14.3		91.0	53.6
Y				12.8		13.7				12.1		3.16		36.2	1.92
Zn				29.3		36.0				18.3		67.1		68.1	–
Zr				97.0		98.2				8.45		4.62		123	89.4
La				12.79		14.5				6.84		2.213		34.53	1.274
Ce				27.19		29.72				4.768		2.039		58.19	1.616
Pr				3.53		3.61				1.29		0.52		7.73	0.261
Nd				13.8		13.87				5.14		2.242		30.95	1.009
Sm				2.69		2.76				1.124		0.449		6.23	0.216
Eu				0.63		0.64				0.315		0.123		1.4	0.046
Gd				2.24		2.47				1.194		0.454		5.48	0.189
Tb				0.351		0.365				0.187		0.068		0.86	0.036
Dy				2.179		2.248				1.198		0.424		5.32	0.19
Ho				0.512		0.507				0.29		0.1		1.19	0.044
Er				1.289		1.3				0.783		0.234		2.94	0.104
Tm				0.203		0.212				0.113		0.038		0.44	0.011
Yb				1.44		1.441				0.769		0.192		2.9	0.078
Lu				0.224		0.26				0.14		0.034		0.45	0.011
$^{87}Sr/^{86}Sr$				–		–				–		0.70873		0.71423	–

(∗) Slate; (∗∗) Biomicrite. LOI: – Loss on ignition at 1100°C.

5. Discussion

5.a. Metamorphic conditions

The absence of minerals such as talc, tremolite and antophylite, common in carbonate metamorphic rocks, may be partly due to the fact that the maximum stability limits for these minerals were surpassed in the carbonatic beds (e.g. for tremolite, the maximum temperature is close to 600 °C). According to Bucher & Frey (1994), at pressures between 1 and 2 kbar, wollastonite can form at 580–610 °C, with maximum stability reached at 730 °C. The diopside + quartz assemblages appear at medium grade intensities and at temperatures greater than 500 °C. Other mineral assemblages with quartz + diopside + wollastonite are formed under the same conditions.

The forsterite + diopsite association indicates that pressure–temperature conditions were 2 kbar and 600–620 °C (Bucher & Frey, 1994). In carbonate rocks with high magnesium content, enstatite is commonly associated with forsterite and diopside. The appearance of spinel also suggests temperatures of 800 °C (Tracy & Frost, 1991). The mineral assemblages of augite–enstatite and quartz, which appear in only one xenolith, represent the highest degree of metamorphism achieved (Bucher & Frey, 1994).

The conditions required to generate complex calcium silicates such as tylleyite, spurrite, rankinite and larnite, however, apparently did not develop, therefore, temperatures of 1000 °C do not seem to have been reached (Winkler, 1976; Bucher & Frey, 1994), at least for a

Table 4. Chemical compositions under microprobe of selected minerals in metamorphic xenoliths (oxides in wt %)

Sample	ANG-96	ANG-96	ANG-96	ANG-37	ANG-37	ANG-9	ANG-9	ANG-100	ANG-121	ANG-96	ANG-96	ANG-37
Mineral	Chrysolite (1)	Chrysolite (2)	Chrysolite (3)	Chrysolite (4)	Forsterite (1)	Forsterite (2)	Forsterite (3)	Forsterite (4)	Forsterite (5)	Diopside	Enstatite (1)	Enstatite (2)
SiO_2	39.727	39.792	38.932	39.519	42.090	41.135	40.443	40.895	40.209	54.981	58.068	56.888
TiO_2	0.060	0.025	0.019	0.024	0.033	0.045	0.000	0.000	0.026	0.069	0.000	0.010
Al_2O_3	0.063	0.030	0.888	0.007	0.000	0.019	0.000	0.010	0.039	0.271	0.051	0.975
FeO	13.610	13.400	10.118	15.110	8.295	7.951	8.731	6.044	7.571	2.511	5.459	7.844
MnO	0.000	0.085	0.069	0.069	0.092	0.043	0.118	0.046	0.012	0.093	0.119	0.026
MgO	46.562	47.085	48.242	45.933	50.854	51.760	50.369	52.682	49.374	18.858	35.182	33.147
CaO	0.212	0.204	0.266	0.116	0.214	0.076	0.560	0.150	0.100	22.523	1.346	1.324
Na_2O	0.038	0.012	0.162	0.040	0.210	0.019	0.027	0.009	–	0.359	0.034	0.179
K_2O	0.030	0.016	0.062	0.013	0.074	0.000	0.009	0.021	–	0.012	0.011	0.009
NiO	0.255	0.304	0.289	0.390	0.439	0.184	0.298	0.399	0.206	0.000	0.040	0.103
Cr_2O_3	0.003	0.006	3.308	0.000	0.009	0.008	0.000	0.000	0.038	0.000	0.000	0.357
Total	100.560	100.959	102.355	101.221	102.310	101.240	100.555	100.256	97.575	99.677	100.310	100.862
Si	0.987	0.984	0.946	0.982	1.002	0.988	0.984	0.985	1.000	1.995	1.992	1.965
Ti	0.001	–	–	–	0.001	0.001	–	–	–	0.002	0.002	–
Al	0.002	0.001	0.025	–	–	0.001	–	–	0.001	0.012	0.157	0.040
Fe	0.283	0.277	0.206	0.314	0.165	0.160	0.178	0.122	0.157	0.076	0.002	0.227
Mn	–	0.002	0.001	0.001	0.002	0.001	0.002	0.001	–	0.003	0.003	0.001
Mg	1.724	1.736	1.747	1.702	1.804	1.853	1.827	1.891	1.830	1.020	1.800	1.787
Ca	0.006	0.005	0.007	0.003	0.005	0.002	0.015	0.004	0.003	0.876	0.049	0.049
Na	0.002	0.001	0.008	0.002	0.010	0.001	0.001	–	–	0.025	0.002	0.012
K	0.001	0.001	0.002	–	0.002	–	–	0.001	–	0.001	–	–
Ni	0.008	0.009	0.009	0.012	0.013	0.006	0.009	0.012	0.006	–	–	0.004
Cr	–	–	0.064	–	–	–	–	–	0.001	–	–	0.010

sufficient length of time for these minerals to have formed.

The data published on tridymite in silica xenoliths related to metamorphic conditions are insufficient to deduce prevailing metamorphic conditions. Zou *et al.* (2004) described metamorphic tridymitic xenoliths with Ce positive anomalies such as those found in sedimentary rocks, but the conditions of temperature and pressure were not established. In the tridymitic xenoliths, silica is not associated with calc-silicate minerals that can help to indicate pressure and temperature conditions. In general, the presence of tridymite implies that these xenoliths underwent and formed at high temperatures, for example, quartz becomes tridymite at $> 870\,^{\circ}$C. (Winkler, 1976; Bucher & Frey, 1994). Wood & Browne (1996) studied a pyrometamorphic magma and found mineral assemblages with tridymite, wollastonite and clinopyroxene formed by quenching after melting between 850 and 1000 °C.

In experimental laboratory work, when the temperature rises to 1050 °C, sedimentary opal CT (interstratifications of disordered low temperature cristobalite and tridymite) (Guthrie, David & Bish, 1995) become ordered α cristobalite (Elzea, Odom & Miles, 1994). From this, it follows that the xenolith α cristobalite would have formed from sedimentary opal CT, and opal A (biogenic) from radiolarites. In the field, and specifically in the case studied, the temperature of formation of α cristobalite would be lower than in the laboratory, probably between 500 and 700 °C, because of its association with wollastonite and diopside. The α cristobalite is metastable below 268 °C and persists at lower temperatures due to strong Si–O bonds.

The mineral assemblages seen in pelitic materials, associated with low-grade metamorphism (temperatures below 300 °C), would seem to have formed in areas furthest from the contact zone, or in contact for only a short time (insufficient for more complete transformations to have occurred).

Results obtained from the study of mineral assemblages of the metasedimentary xenoliths indicate that a wide range of temperatures led to assemblages of low, medium and high grade. Nevertheless, the majority of the xenoliths may indicate temperatures from 600 to 900 °C and pressures of less than 2 kbar. These are the conditions which would prevail in a small magmatic chamber at a depth of 4 km, as deduced by Ortiz *et al.* (1986). The small size of this chamber may be due to its formation from a widening of the conduit, where eruption would be temporarily detained.

5.b. Forsteritic xenoliths

Although this paper does not attempt to revise the origin of ultrabasic xenoliths, which other authors place in the mantle (Sagredo, 1969; Neumann *et al.* 1995), the forsterite with undulose extinction (Fig. 5b) found in some metasedimentary xenoliths, and the forsterite, scapolite and augite (Table 5) in xenoliths with macrocrystalline forsterite could lead one to consider a possible cogenesis of ultrabasic and metamorphic xenoliths. However, there is another possibility, namely that because scapolite (which normally forms at temperatures above 800 °C) can form at 500 °C in the presence of an excess of sodium (Newton, Charlu & Kleppa, 1980), and as the scapolite detected was in the form of microcrystals occupying the spaces between

Table 4. (cont.)

Sample	ANG-9	ANG-46	ANG-96	ANG-37	ANG-9	ANG-9	ANG-9	ANG-121	ANG-37	ANG-121	ANG-97	ANG-97
Mineral	Wollasto-nite 2M	Wollasto-nite	Chromite (1)	Chromite (2)	Chromite (3)	Chromite (4)	Chromite (5)	Chromite (6)	Quartz	Scapolite (1)	Scapolite (2)	Ortho-clase
SiO_2	56.887	42.62	1.007	0.062	0.058	0.000	0.031	0.051	98.697	62.775	57.642	63.555
TiO_2	0.219	0.017	0.317	0.206	0.049	0.108	0.143	0.069	0.000	1.045	0.768	0.083
Al_2O_3	6.049	7.04	8.342	20.541	23.589	21.105	18.372	11.959	0.000	16.963	16.639	18.449
FeO	0.752	1.34	23.275	21.077	21.946	13.890	18.949	17.540	0.018	2.774	2.994	0.073
MnO	0.000	0.09	0.256	0.223	0.126	0.127	0.213	0.235	0.063	0.057	0.010	0.000
MgO	0.968	8.57	11.258	16.042	9.9980	15.372	15.094	14.182	0.000	1.374	1.753	0.005
CaO	33.543	38.75	0.098	0.020	0.001	0.000	0.019	0.010	0.074	4.408	11.989	0.380
Na_2O	1.138	1.92	0.381	0.000	0.000	0.000	0.000	–	0.019	4.249	1.421	1.541
K_2O	0.693	0.17	0.215	0.000	0.002	0.003	0.000	0.014	0.003	3.483	4.101	13.991
NiO	0.000	–	0.052	0.185	0.050	0.069	0.174	0.038	0.000	0.013	0.080	0.057
Cr_2O_3	0.000	0.01	50.182	41.640	43.932	49.330	48.119	54.859	0.000	0.021	0.020	0.000
Total	100.249	100.059	95.383	99.996	99.733	100.004	101.114	98.957	98.874	97.162	97.417	98.134
Si	6.230	1.648	0.283	0.015	0.011	–	0.008	0.013		2.182	10.983	11.986
Ti	0.018	–	0.067	0.039	0.007	0.020	0.027	0.014		0.027	0.110	0.012
Al	0.781	0.321	2.762	6.047	5.471	6.090	5.388	3.682		0.695	3.737	4.873
Fe	0.069	0.043	5.469	4.403	3.537	2.844	3.943	3.832		0.081	0.477	0.011
Mn	–	0.003	0.061	0.047	0.021	0.026	0.045	0.052		0.002	0.002	–
Mg	0.158	0.494	4.715	5.973	2.933	5.610	5.600	5.523		0.071	0.498	0.001
Ca	3.936	1.605	0.030	0.005	–	–	0.005	0.003		0.164	2.448	0.076
Na	0.242	0.144	0.208	–	–	–	–	–		0.286	0.525	0.560
K	0.097	–	0.077	–	0.001	0.001	–	0.005		0.154	0.007	3.344
Ni	–	–	0.018	0.058	0.012	0.021	0.055	0.013		0.001	0.019	0.013
Cr	–	–	11.147	8.223	11.502	9.549	9.467	11.332		0.001	0.003	–

Formula of: pyroxenes with 6 oxygens (wollastonite and wollastonite 2M, 18 oxygens); feldspars 32 oxygens; chromite 32 oxygens; olivine 4 oxygens; scapolite 24 oxygens

Table 5. Chemical composition of selected minerals in forsteritic xenoliths

Sample	11131	10507	10507	10507
Mineral	Forsterite	Forsterite	Scapolite	Augite
SiO_2	41.080	42.546	54.989	50.332
TiO_2	0.010	–	0.834	0.206
Al_2O_3	0.028	0.075	21.973	3.397
FeO	7.996	7.228	5.251	2.958
MnO	0.096	0.033	0.020	0.012
MgO	50.92	49.863	0.609	17.142
CaO	0.015	0.021	3.714	20.696
Na_2O	–	–	6.488	0.622
K_2O	–	0.013	4.982	0.029
NiO	0.307	0.226	0.121	0.033
Cr_2O_3	–	–	0.017	3.257
Total	100.46	100.096	98.998	98.684
Si	0.994	1.026	1.952	1.867
Ti	–	–	0.022	0.006
Al	0.001	0.002	0.920	0.149
Fe	0.0162	0.146	0.156	0.092
Mn	0.002	0.001	0.001	–
Mg	1.837	1.792	0.032	0.948
Ca	–	0.001	0.141	0.823
Na	–	–	0.446	0.045
K	–	–	0.226	0.001
Ni	0.009	0.007	0.005	0.002
Cr	–	–	–	0.096

pyroxenes and olivines, such scapolite may be a metasomatic mineral produced in the mantle or through contact between dunite xenoliths and host lava.

5.c. Contamination

Contamination of Canary Island volcanic rocks by crustal sedimentary rocks has been cited by various authors. Demeny *et al.* (2000) refer to carbonatites from Fuerteventura contaminated by sediments. Gurenko, Chaudisson & Schmincke (2001), found basalts contaminated by oceanic sediments from a bore-hole in southwestern Gran Canaria. Troll & Schmincke (2002), in a detailed study of the isotopic composition of basalts and xenoliths from the oceanic crust in Gran Canaria, deduce that there was no magmatic differentiation, nor genesis of basalts at varying depths, but contamination by crustal rocks. Hansteen & Troll (2003) explain that shield basalts (old series) from Gran Canaria may originate by assimilation of oceanic crust and do not necessarily reflect mantle characteristics.

Variuos authors have identified contamination by unidentified crustal rocks in Lanzarote (e.g. Lindstrom, Hoernle & Gill, 2003). Only Araña & Bustillo (1992) associate the large number of sedimentary xenoliths, rich in SiO_2, with contamination of magma in the lavas emitted during the final period of the 1730–1736 eruption.

The IGPETWIN-MIXING program (Carr, 1994) was used to verify and quantify the contamination process of the initial basanitic magma, typical of Canary Island magmatism, by sedimentary or metamorphic host rocks. Typical basanites from the Timanfaya eruption with silica content between 41 and 42 % (Carracedo & Rodríguez-Badiola, 1991) were chosen as parent 1. Various combinations of calc-silicate and silica xenoliths were used as parent 2. Anomalous basalts with high silica content (47–51 %: Carracedo & Rodríguez-Badiola, 1991) should be the resulting

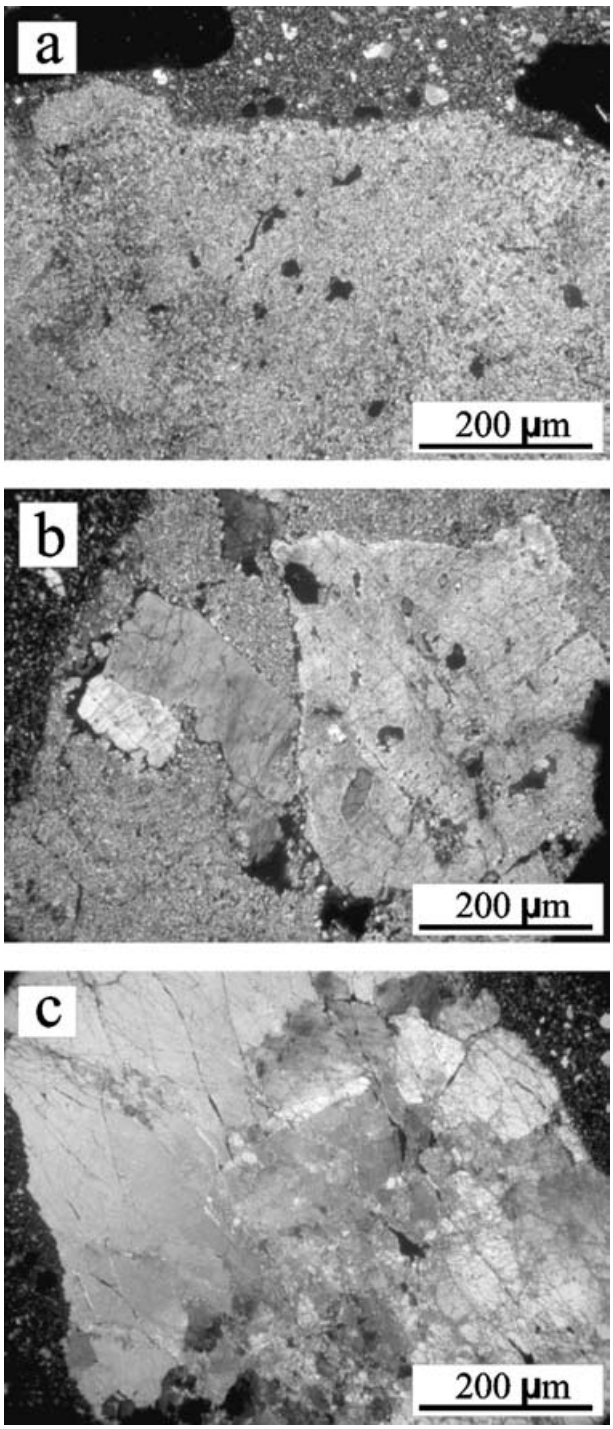

Figure 5. Photographs of diverse textures, from thin-section and crossed nicols, of the fosteritic xenoliths, showing different stages of crystallization. (a) Microcrystalline texture. (b) Phenocrysts of forsterite included in a microcrystalline groundmass. (c) Macrocrystalline xenolith.

hybrid rocks. The results are shown in Table 6, where the sum of the squares of the residuals gives acceptable values for mixing.

Possible contamination can also be shown through studied REE content of xenoliths and volcanic rocks. Figure 7 shows that the REE contents of Timanfaya basalts are the lowest, compared with REE content of

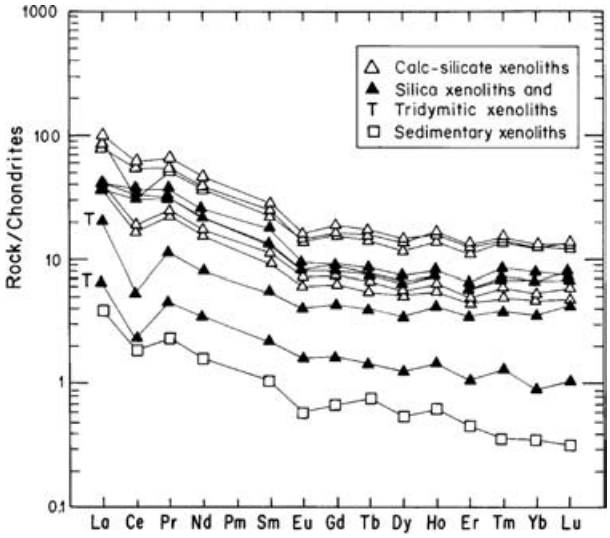

Figure 6. REE model for the calc-silicate, silica metamorphic and sedimentary xenoliths in the lavas of the Timanfaya eruption.

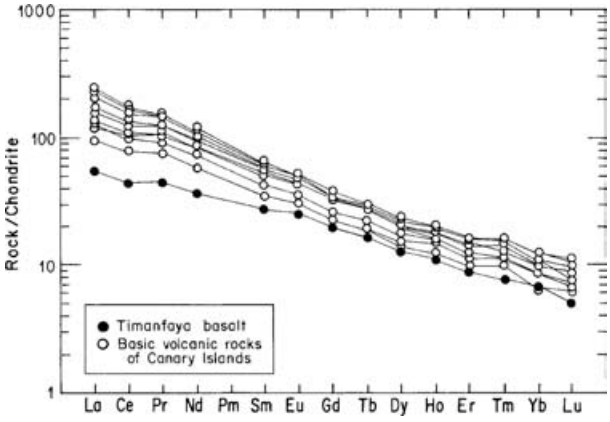

Figure 7. REE model of Timanfaya basalt superimposed on the REE model for the basic volcanic rocks of the Canaries (Aparicio *et al.* 2003), showing that the LREE contents of the Timanfaya basalt are the lowest.

the main Canary Island basic rocks (Aparicio *et al.* 2005). Moreover, the REE content of Timanfaya basalts fits with that of the metasedimentary xenoliths from the same zone, also with a weak Ce anomaly.

6. Conclusions

Underneath the Island of Lanzarote, a process of contact metamorphism transformed sedimentary rocks of varying nature (limestones, mudstones, dolomites, sandstones, etc.) into metamorphic rock with mineral assemblages corresponding to various temperatures.

(1) The upper temperature limit could be marked by the formation of tridymite coming from the metamorphism of sedimentary series with radiolarites. These temperatures would have been above 870 °C, the point of phase change of quartz to tridymite, but should not have reached 1000 °C, as there are no complex

Table 6. Examples of basanitic magma mixing with metasedimentary xenoliths

Parent 1 Volcanic rock	Parent 2 Metasedimentary xenoliths	Hybrid Volcanic rock	Sum of the squares of residuals
E1 (41.85) BS	ANG-83 si	M11 BA (47.05)	0.241
ML1 (41.14) BS	ANG-20 si		
ML3 (42.06) BS	ANG-31 si		
E3 (41.54) BS	ANG-29 ca		
E1 (41.85) BS	ANG-11 ca	M42 BA (46.85)	0.634
ML1 (41.14) BS	ANG-73 ca		
ML3 (42.06) BS	ANG-64 ca		
E3 (41.54) BS	ANG-46 ca		
E1 (41.85) BS	ANG-89 si	M-25 BA (49.76)	1.59
ML.1 (41.14) BS	ANG-86 si		
ML3 (42.06) BS	ANG-19 si		
E3 (41.54) BS	ANG-100 si		
E1 (41.85) BS	ANG-39 si	M-31 BA (50.26)	0.415
ML.1 (41.14) BS	ANG-26 si		
ML.3 (42.06) BS	ANG-74 si		
E3 (41.54) BS	ANG-87 si		
E1 (41.85) BS	ANG-39 si	M-25 BA (49.76)	0.35
ML.1 (41.14) BS	ANG-26 si		
ML.3 (42.06) BS	ANG-74 si		
E3 (41.54) BS	ANG-87 si		
E1 (41.85) BS	ANG-39 si	M-41 BA (50.15)	0.62
ML.1 (41.14) BS	ANG-26 si		
ML.3 (42.06) BS	ANG-74 si		
E3 (41.54) BS	ANG-87 si		
E1 (41.85) BS	ANG-39 si	MC-1 BA (49.28)	0.35
ML.1 (41.14) BS	ANG-26 si		
ML.3 (42.06) BS	ANG-74 si		
E3 (41.54) BS	ANG-87 si		
E1 (41.85) BS	ANG-39 si	M-31 BA (50.26)	0.416
ML1 (41.14) BS	ANG-74 si		
ML3 (42.06) BS	ANG-87 si		
E3 (41.54) BS	ANG-19 si		
E1 (41.85) BS	ANG-39 si	M-25 BA (49.76)	0.36
ML1 (41.14) BS	ANG-74 si		
ML3 (42.06) BS	ANG-87 si		
E3 (41.54) BS	ANG-19 si		
E1 (41.85) BS	ANG-39 si	M-41 BA (50.15)	0.58
ML1 (41.14) BS	ANG-74 si		
ML3 (42.06) BS	ANG-87 si		
E3 (41.54) BS	ANG-19 si		
E1 (41.85) BS	ANG-39 si	MC-1 BA (49.88)	0.87
ML1 (41.14) BS	ANG-74 si		
ML3 (42.06) BS	ANG-87 si		
E3 (41.54) BS	ANG-19 si		
E1 (41.85) BS	ANG-41 si	M-25 BA (49.76)	1.06
ML1 (41.14) BS	ANG-58 si		
ML3 (42.06) BS	ANG-87 si		
E3 (41.54) BS	ANG-81 si		
E1 (41.85) BS	ANG-11 si	M-25 BA (49.76)	1.06
ML1 (41.14) BS	ANG-42 si		
ML3 (42.06) BS	ANG-81 si		
E3 (41.54) BS	ANG-87 si		

Samples E-1, E-3, M-3, M-11, ML-1, ML-3, M-42, M-31, M-25, M-41 and MC-1 from Carracedo & Rodríguez Badiola (1991). BA – Basalt; BS – Basanite; ca – calc-silicate xenoliths; si – silica xenoliths. Numbers in brackets represents SiO_2 content in wt %.

calcic silicates. This metamorphism took place at less than 2 kbar pressure, at some 4–5 km depth, and affected Paleocene and earlier sediments.

(2) This metamorphism is probably due to a shallow magma reservoir (1200 °C) formed during the volcanic process that gave rise to the 1730–1736 Timanfaya eruptions.

(3) The metamorphic gradient observed in the xenoliths is possibly due to the distance of the sedimentary rocks from the magma chamber and

position (beside or above) relative to it. This would explain the scarcity of low-grade samples that would correspond to sediments further from the chamber and conduits.

(4) Some sedimentary strata rich in silica, such as the radiolarites, located near the intrusion, could have melted completely and mixed with the magma, contaminating it with silica.

(5) 'Anomalies' in some metamorphic mineral compositions could be related to the basic nature of the intruding magma and the fact that contact metamorphism was not originated by acid (granitic) rocks, as described in current publications.

(6) Diffusion from the chamber to the sedimentary surrounding rock would explain its enrichment in REE (relative to sediments unaffected by metamorphism) and the increase in REE in the erupted basalt relative to the typical composition of Canary Island Basalts.

(7) Identical metamorphic and ultrabasic xenolith textures and mineralogies point to a possible metamorphic origin for some ultrabasic xenoliths.

Acknowledgements. We are grateful to Orlando Hernandez for providing some of the samples studied. This work was partially financed by the projects "Aspectos Educativos del Volcanismo Canario" (FEDER) and National Project BTE 2002-04017-CO2-1. A M. Vallejo y M.I. Ruiz por los trabajos analíticos. We are also especially grateful to the Geological Magazine reviewers Drs L. E. Thomas and V. R. Troll, for their helpful suggestions and constructive comments. We thank M. C. Sendra, J. Arroyo, M. Castillejo and J. M. Hontoria for their assistance in various areas of this work.

References

Aparicio, A., Hernán, F., Cubas, C. R. & Araña, V. 2003. Los magmas mantélicos y evolución del volcanismo canario. *Estudios Geológicos* **59**, 5–14.

Aparicio, A., Araña, V., Hernán, F. & Cubas, C. R. 2005. *Litotipos de las Islas Canarias*. Casa de Los Volcanes, Cabildo de Lanzarote, 73 pp.

Araña, V. & Bustillo, M. A. 1992. Volcanologic concerns of the siliceous metasedimentary xenoliths included in historic lava-flows of Lanzarote (Canary Islands). *Acta Volcanológica* **2**, 1–6.

Araña, V. & Ortiz, R. 1991. The Canary Islands: Tectonic, Magmatism and Geodynamic Framework. In *Magmatism in extensional structural settings, the Phanerozoic African Plate* (eds A. B. Kampunzu and R. T. Lubala), pp. 209–49. Berlin: Springer-Verlag.

Banda, E., Dañobeitia, J. J., Suriñach, E. & Ansorge, J. 1981. Features of crustal structure under the Canary Islands. *Earth and Planetary Science Letters* **55**, 11–24.

Banda, E., Ranero, C. R., Dañobeitia, J. J. & Rivero, A. 1992. Seismic boundaries of the eastern central Atlantic Mesozoic crust from multichannel seismic data. *Geological Society of America Bulletin* **104**, 1340–9.

Brandle, J. L. & Fernández-Santín, S. 1979. On the non-existence of a tholeitic series in the Canary Islands. *Chemical Geology* **26**, 91–103.

Bucher, K. & Frey, M. 1994. *Petrogenesis of metamorphic rocks*. New York: Springer-Verlag, 318 pp.

Bustillo, M. A., Nishimura, A., Araña, V. & Hattori, I. 1994. Paleocene radiolarians from xenoliths hosted in Holocene lavas of Lanzarote (Canary Islands). *Geobios* **27**, 181–8.

Carbonin, S. & Menegazzo, G. 1996. Teaching application of an x-ray powder diffraction data card file: XRD profile simulation and hanawalt index tabulation. *Computer Geosciences* **22**, 935–42.

Carr, M. J. 1994. *IGPETWIN: Igpet for Windows petrology software*. Somerset: Terra Softa.

Carracedo, J. C. & Rodríguez-Badiola, E. 1991. *Lanzarote. La erupción volcánica de 1730*. CSIC-Estación Volcanológica de Canarias, 184 pp.

Collier, J. S. & Watts, A. B. 2001. Lithospheric response to volcanic loading by the Canary Islands: constraints from seismic reflection data in their flexural moat. *Journal of Volcanology and Geothermal Research* **147**, 660–76.

Deer, W. A., Howie, R. A. & Zussman, J. 1992. *An introduction to the rock-forming minerals*. Edinburgh: Pearson Prentice Hall, 696 pp.

Demeny, A., Ahijado, A., Casillas, R., Boyce, A. J. & Fallick, A. E. 2000. Crustal contamination of carbonatites indicated by $\delta^{34}S$–$\delta^{13}C$ correlations (Fuerteventura, Canary Islands). *Revista Sociedad Geológica de España* **12**, 453–60.

De Ros, L. F., Morad, S. & Al-Aasm, I. S. 1997. Diagenesis of siliciclastic and volcanoclastic sediments in the Cretaceous and Miocene sequences of the NW African margin (DSDP Leg 47 A, site 397). *Sedimentary Geology* **112**, 137–56.

Elzea, J. M., Odom, I. E. & Miles, W. J. 1994. Distinguishing well-ordered opal-CT and opal-C from high-temperature cristobalite by X-ray diffraction. *Analythica Chimica Acta* **286**, 107–16.

Fleet, A. J. 1984. Aqueous and sedimentary geochemistry of the rare earth elements. In *Rare Earth element geochemistry* (ed. P. Henderson), pp. 343–73. Elsevier.

Fuster, J. M., Cendrero, A., Gastesi, P., Ibarrola, E. & López-Ruiz, J. 1968. *Geología y Volcanología de las Islas Canarias*. Fuerteventura, ILM-CSIC Madrid, 239 pp.

Govindaraju, K. & Mevelle, G. 1987. Fully automated dissolution and separation methods for inductively coupled plasma atomic emission spectrometry rock analysis-application to the determination of rare elements. *Journal of Analytical Atomic Spectrometry* **2**, 615–21.

Gurenko, A. A., Chaudisson, M. & Schmincke, H. U. 2001. Magma ascent and contamination beneath one intraplate volcano: evidence from S and O isotopes in glass inclusions and their host clinopyroxene from Miocene basaltic hyaloclastites southwest of Gran Canaria (Canary Islands). *Geochimica et Cosmochimica Acta* **64**, 4359–74.

Guthrie, G. D., David, J. R. & Bish, D. L. 1995. Modeling the X-ray diffraction pattern of opal-CT. *American Mineralogist* **80**, 869–72.

Hansteen, T. H. & Troll, V. R. 2003. Oxygen isotope composition of xenoliths from the oceanic crust and volcanic edifice beneath Gran Canaria (Canary Islands): consequences for crustal contamination of ascending magmas. *Chemical Geology* **193**, 181–93.

Heaney, P. J. & Post, J. E. 1992. The widespread distribution of a novel silica polymorph in microcrystalline quartz varieties. *Science* **255**, 441–3.

IBARROLA, E. & LÓPEZ RUIZ, J. 1967. Estudio petrológico y químico de las erupciones recientes (Serie IV) de Lanzarote (Islas Canarias). *Estudios Geológicos* **23**, 203–13.

IBARROLA, E. 1970. Variabilidad de los magmas basálticos en las Canarias Orientales y Centrales. *Estudios Geológicos* **26**, 337–400.

JAROSEWICH, E. J., NELEN, J. A. & NORBERG, J. A. 1980. Reference samples for electron microprobe analysis. *Geostandards Newsletter* **4**, 43–7.

KRASTEL, S. & SCHMINCKE, H. V. 2002. Crustal structure of northern Gran Canaria, Canary Islands, deduced from active seismic tomography. *Journal of Volcanology and Geothermal Research* **115**, 153–77.

LINDSTROM, C. C., HOERNLE, K. & GILL, J. 2003. U-series disequilibria in volcanic rocks from the Canary Islands, plume versus lithospheric melting. *Geochimica et Cosmochimica Acta* **67**, 4155–78.

MARTÍNEZ, W. & BUITRAGO, J. 2002. Sedimentación y volcanismo al este de las islas de Fuerteventura y Lanzarote (Surco de Fuster Casas). *Geogaceta* **32**, 51–4.

NEUMANN, E. R., WULFF-PEDERSEN, E., JOHNSEN, K., ANDERSEN, T. & KROGH, E. 1995. Petrogenesis of spinel harzburgite and dunite suite xenoliths from Lanzarote, eastern Canary Islands: implications for the upper mantle. *Lithos* **35**, 83–107.

NEWTON, R. C., CHARLU, T. V. & KLEPPA, O. J. 1980. Thermochemistry of the high structural state plagioclases. *Geochimica et Cosmochimica Acta* **44**, 933–41.

ORTIZ, R., ARAÑA, V. & VALVERDE, C. 1986. Aproximación al conocimiento del mecanismo de la erupción de 1730–1736 en Lanzarote. *Anales de Física Serie B. Special Issue* "Física de los Fenómenos Volcánicos", 127–42.

ORTIZ, R., ARAÑA, V., ASTIZ, M. & GARCIA, A. 1986. Magnetotelluric study of the Teide (Tenerife) and Timanfaya (Lanzarote) volcanic areas. *Journal of Volcanology and Geothermal Research* **30**, 357–77.

RANERO, C. R. & BANDA, E. 1997. The crustal structure of the Canary Basin: Accretion processes at slow spreading centers. *Journal of Geophysical Research* **102**(B5), 10185–201.

RENZ, O., BERNOULLI, D. & HOTTINGER, L. 1992. Cretaceous ammonites from Fuerteventura, Canary Islands. *Geological Magazine* **129**, 763–9.

RICHARD, P., SHIMIZU, N. & ALLEGRE, C. J. 1976. $^{143}Nd/^{144}Nd$, a natural tracer: an application to oceanic basalts. *Earth and Planetary Science Letters* **31**, 269–78.

ROBERTSON, A. H. F. & BERNOULLI, D. 1982. Stratigraphy, facies, and significance of Late Mesozoic and Early Tertiary Sedimentary Rocks of Fuerteventura (Canary Islands) and Maio (Cape Verde Islands). In *Geology of the Northwest African Margin* (eds U. von Rad, K. Hinz, M. Sarnthein and E. Seibold), pp. 498–525. Springer Verlag.

SAGREDO, J. 1969. Origen de las inclusiones de dunitas y otras rocas ultramáficas en las rocas volcánicas de Lanzarote y Fuerteventura. *Estudios Geológicos* **25**, 189–233.

SÁNCHEZ GUZMÁN, J. & ABAD, J. 1986. Sondeo Geotérmico Lanzarote-1. Significado geológico y geotérmico. *Anales de Física* Serie B **82**, Special Issue, 102–9.

SCHMINCKE, H. U., KLUGEL, A., HANSTEEN, T. H., HOERNLE, K. & BOGARD, P. VAN DEN. 1998. Samples from the Jurassic ocean crust beneath Gran Canaria, La Palma and Lanzarote (Canary Islands). *Earth and Planetary Science Letters* **163**, 343–60.

SIGMARSSON, O., CARN, S. & CARRACEDO, J. C. 1998. Systematics of U-series nuclides in primitive lavas from the 1730–36 eruption on Lanzarote, Canary Islands and implications for the role of garnet pyroxenites during oceanic basalt formations. *Earth and Planetary Science Letters* **162**, 137–51.

SMITH, J. V. & STEELE, I. M. 1984. Chemical substitution in silica polymorphs. *Neues Jahrbuch für Mineralogie, Monatshefte* **H.3**, 137–44.

STILLMAN, C. J., FUSTER, J. M., BENNELL-BAKER, M. J., MUÑOZ, M. J., SMEWING, J. D. & SAGREDO, J. 1975. Basal Complex of Fuerteventura is an oceanic intrusive complex with rift system affinities. *Nature* **257**, 469–71.

SURIÑACH, E. 1986. La estructura cortical del Archipiélago Canario, resultados de la interpretación de perfiles sísmicos profundos. *Anales de Física Serie* B **82**, Special Issue, 62–7.

THOMAS, L. E., HAWKESWORTH, C. J., VAN CARLSTEREN, S. P., TURNER, S. P. & ROGERS, N. W. 1999. Melt generation beneath ocean islands: a U–Th–Ra isotope study from Lanzarote in the Canary Islands. *Geochimica et Cosmochimica Acta* **63**, 4081–99.

TRACY, R. J. & FROST, B. R. 1991. Phase equilibria and thermobarometry of metapelites. *Review of Mineralogy* **26**, 207–80.

TROLL, V. T. & SCHMINCKE, H. U. 2002. Magma mixing and crustal recycling recorded in ternary feldspar from compositionally zoned peralkaline ignimbrite "A", Gran Canaria, Canary Islands. *Journal of Petrology* **43**, 243–70.

WATTS, A. B. 1994. Crustal structure, gravity anomalies and flexure of the lithosphere in the vicinity of the Canary Islands. *Geophysical Journal International* **119**, 648–66.

WATTS, A. B., PIERCE, C., COLLIER, J., DALWOOD, R., CANALES, J. P. & HENSTOCK, T. J. 1997. A seismic study of lithospheric flexure in the vicinity of Tenerife, Canary Islands. *Earth and Planetary Science Letters* **146**, 431–47.

WINKLER, H. G. F. 1976. *Petrogenesis of metamorphic rocks. New York*: Springer-Verlag, 334 pp.

WOOD, C. P. & BROWNE, P. R. L. 1996. Chlorine-rich pyrometamorphic magma at White Island volcano, New Zealand. *Journal of Volcanology and Geothermal Research* **72**, 21–35.

ZOU, H., MCKEEGAN, K. D., XU, X. & ZINDLER, A. 2004. Fe–Al-rich tridymite-hercynite xenoliths with positive cerium anomalies: preserved lateritic paleosols and implications for Miocene climate. *Chemical Geology* **207**, 101–16.